Short-range correlations and the $3s_{1/2}$ wave function in ^{206}Pb

M. R. Anders,[1] S. Shlomo,[1,2] and I. Talmi[2]
[1]*Cyclotron Institute, Texas A&M University, College Station, Texas 77840, USA*
[2]*The Weizmann Institute of Science, Rehovot 76100, Israel*
(Received 15 July 2015; revised manuscript received 20 August 2015; published 17 September 2015)

The charge-density difference between ^{206}Pb and ^{205}Tl, measured by elastic electron scattering, offers a unique opportunity to look for effects of short-range correlations on a shell-model wave function of a single proton. The measured difference is very similar to the charge density due to a proton in a $3s_{1/2}$ orbit. If there is a potential whose $3s_{1/2}$ wave function yields the measured difference between the charge distributions, no effect of short-range correlations is evident. To check this point, we look for a potential whose $3s_{1/2}$ wave function yields the measured data. We developed a novel method to obtain the potential directly from the density and its first and second derivatives. Fits to parametrized potentials were also carried out. The $3s_{1/2}$ wave functions of the potentials determined here reproduce fairly well the experimental data within the quoted errors. To detect possible effects of two-body correlations on the $3s_{1/2}$ shell-model wave function, more accurate measurements are required.

DOI: 10.1103/PhysRevC.92.034318 PACS number(s): 21.60.Cs, 21.10.Gv, 25.30.Bf, 27.80.+w

I. INTRODUCTION

An important problem is how the success of the nuclear shell model can be reconciled with the strong and short-ranged interaction between free nucleons. It was realized that shell-model wave functions are eigenstates of a *renormalized* nuclear Hamiltonian in which the interactions are rather tame. Thus, shell-model wave functions of independently moving nucleons do not have short-range correlations. The latter are imposed on the *real* wave functions by the strong short-range interaction between free nucleons (the bare interaction). According to current results of the nuclear many-body theory, short-range two-nucleon correlations due to the bare interaction play an important role. In some papers, the admixtures into shell-model wave functions due to correlations were calculated to be rather high, up to 35% [1,2].

Still, there are indications that shell-model wave functions have a certain reality. A possible way to check it was to measure the difference between charge distributions of two nuclei with the same N and $Z_2 = Z_1 - 1$ [3]. A much higher accuracy was obtained in the experiment of Refs. [4,5] for the difference between the charge densities of ^{206}Pb and ^{205}Tl. The authors used elastic electron scattering. The difference between the charge distributions which they determined is very similar to the one due to a proton wave function in a $3s_{1/2}$ orbit. It has a clear maximum at the origin and two additional maxima. This result is in agreement with the simple shell model. The $\frac{1}{2}^+$ ground state of ^{205}Tl shows that the $3s_{1/2}$ orbit is the highest in the proton $Z = 82$ major shell. The authors noticed that the experimental charge density near $r = 0$ is much lower than the one due to a Hartree-Fock calculation and to the one obtained from a conventional Woods-Saxon (WS) single-particle potential. They attributed it to a rather strong (30%) admixture of a shell-model wave function in which the proton hole is in a $2d_{3/2}$ state, coupled to a $J = 2$ state of two neutron holes [4,5]. As pointed in Ref. [6], the inclusion of the $2d_{3/2}$ orbital leads to an agreement with data at the origin, but deviations from data by a factor of 2 occur in the region between 2 and 4 fm. An attempt to obtain the observed shape of the charge distribution from a conventional Woods-Saxon potential was carried out in Ref. [6]. The authors assumed a significant modification of the proton form factor (increasing the charge radius) in medium. This assumption was also made to explain the European Muon Collaboration (EMC) effect. However, it was shown in Ref. [7] that the EMC effect was simply explained by the fact that nucleons are bound in a nucleus. One should use the four-momenta distribution function in calculating the deep inelastic muon (electron) cross section on a nucleus.

A large deviation from the shell-model wave function has direct implications to direct nuclear reactions. Results of these reactions depend on the occupation probability of shell-model orbits. The estimates obtained by analysis of experimental data are usually less than those expected from the shell model. Such estimates are based on measured cross sections of various reactions which seem to be smaller than those calculated with shell-model wave functions. Unlike the depletions which are considered in those reactions, the measured ^{206}Pb-^{205}Tl charge difference is *exactly* equal to one proton charge. Any effect of short-range correlations could only modify the *shape* of the difference between the charge distributions. The striking results of the measured difference of the charge densities [4,5] deserve attention. In the present paper, we look for a potential whose proton $3s_{1/2}$ wave function can reproduce the measured difference.

If such a potential exists, no effect of short-range correlations is evident in the experimental data. This would definitely not contradict the existence of those correlations. The latter cause "wounds" in shell-model wave functions. If the wound occupies a small volume, it will not have a big effect on expectation values of "long-range" operators. This term was used in a paper on *ab initio* calculations [8]. The authors consider short-range and long-range operators. They find that "when the operator becomes long range, the renormalized operator becomes indistinguishable from the bare value."

This means that for long-range operators, shell-model wave functions may be safely used.

If a potential as described above is found, it could serve also as an additional constraint in the determination of a modern energy density functional for a more reliable prediction of properties of nuclei and nuclear matter [9,10].

We developed a new method to determine the single-particle potential directly from the single-particle matter density and its first and second derivatives. In Sec. II we consider the single-particle Schrödinger equation and describe the method for determining the single-particle potential $V(\vec{r})$ from a given single-particle wave function $\psi(\vec{r})$ or matter density $\rho(\vec{r})$, assuming it is known for all $\vec{r}$. In particular, we consider the case of spherical symmetry. We also describe the method of deducing the point proton density directly from the charge distribution determined in electron-scattering measurements. In Sec. III we present our attempts to construct a single nucleon potential whose $3s_{1/2}$ proton wave function yields a good fit to the data. The experimental data [4,5] are for the charge-density difference between the close ($\Delta Z = 1$) isotones ^{206}Pb-^{205}Tl. In Sec. IV we present our conclusions.

II. FORMALISM

Consider the single-particle Schrödinger equation,

$$-\frac{\hbar^2}{2m}\Delta\psi + V\psi = E\psi, \tag{1}$$

where $V(\vec{r})$ is a real local and nonsingular potential. From Eq. (1) follows that for a given single-particle wave function $\psi(\vec{r})$, known for all $\vec{r}$, and given eigenvalue E, the corresponding single-particle potential V is uniquely determined by

$$V(\vec{r}) = E + \frac{\hbar^2}{2m}S(\vec{r}), \qquad S(\vec{r}) = \frac{\Delta\psi(\vec{r})}{\psi(\vec{r})}. \tag{2}$$

For a nonsingular V, $\Delta\psi(\vec{r}) = 0$ when $\psi(\vec{r}) = 0$. The relation for $[\psi(\vec{r})]^b$, where b is a positive integer, is given in Ref. [11]. In the present paper we consider the spherically symmetric case where

$$\psi_{nlj}(\vec{r}) = \frac{R_{nlj}(r)}{r}Y_{lj}. \tag{3}$$

Here, $R_{nlj}(r)$ is the radial wave function for the orbit with principal number n, orbital angular momentum l, and total angular momentum j, and Y_{lj} is the eigenfunction of the angular momenta l and j. In the following we limit the discussion to the proton $3s_{1/2}$ orbit. Therefore, the corresponding single-particle potential for a nucleon is

$$\begin{aligned} V_{\rm cen}(r) &= E + \frac{\hbar^2}{2m}S(r) - \frac{1}{2}(1-\tau_z)V_{\rm Coul}(r), \\ S(r) &= \frac{1}{R_{nlj}(r)}\frac{d^2R_{nlj}}{dr^2}, \end{aligned} \tag{4}$$

where $V_{\rm cen}(r)$ and $\frac{1}{2}(1-\tau_z)V_{\rm Coul}(r)$ are the central and Coulomb potentials, respectively. Here, $\tau_z = 1$ for a neutron and -1 for a proton.

The single-particle radial density $\rho_{nlj}(r)$ is related to the square of the radial wave function R^2_{nlj} by

$$R^2_{nlj}(r) = 4\pi r^2\rho_{nlj}(r). \tag{5}$$

From (5) it is possible to extract the wave function $R_{nlj}(r)$ and use Eq. (4) to deduce the corresponding single-particle potential, but this leads to additional complications. Therefore, we developed a method to determine the potential directly from the density and its first and second derivative. Using Eq. (4), we obtain the simple relation with R^2_{nlj},

$$S(r) = \frac{1}{2R^2_{nlj}}\left\{\frac{d^2\left(R^2_{nlj}\right)}{dr^2} - \frac{1}{2}\frac{1}{R^2_{nlj}}\left[\frac{d\left(R^2_{nlj}\right)}{dr}\right]^2\right\}. \tag{6}$$

When $R^2_{nlj} = 0$, $dR^2_{nlj}/dr = 0$ with the additional condition that the term on the right-hand side of Eq. (6) in the curly brackets also vanishes. From Eqs. (5) and (6) we find the relation,

$$S(r) = \frac{1}{2\rho_{nlj}}\left[\frac{d^2\rho_{nlj}}{dr^2} + \frac{2}{r}\frac{d\rho_{nlj}}{dr} - \frac{1}{2\rho_{nlj}}\left(\frac{d\rho_{nlj}}{dr}\right)^2\right]. \tag{7}$$

When $\rho_{nlj} = 0, d\rho_{nlj}/dr = 0$ with the additional condition that the term $\frac{d^2\rho_{nlj}}{dr^2}$ also vanishes.

A commonly used central nuclear potential is the WS potential,

$$V(r) = V_0/\{1 + \exp[(r - R_1)/a_0]\}, \tag{8}$$

where, V_0, R_1, and a_0 are the depth, half radius, and diffuseness parameters, respectively. For the Coulomb potential we adopt the form obtained from a uniform charge distribution of radius $R_{\rm ch}$,

$$V_{\rm Coul}(r) = Ze^2\begin{cases}\left(3 - r^2/R^2_{\rm ch}\right)/2R_{\rm ch}, & r < R_{\rm ch},\\ 1/r, & r > R_{\rm ch},\end{cases} \tag{9}$$

with $R^2_{\rm ch} = (5/3)\langle r^2\rangle_{\rm ch}$, where $\langle r^2\rangle_{\rm ch}$ is the charge mean-square radius.

In elastic electron-nucleus scattering measurements the charge-density distribution $\rho_{\rm ch}(\vec{r})$ is determined by carrying out a phase-shift analysis of the cross section [12]. In theoretical models the point proton density distribution $\rho_p(\vec{r})$ is calculated. The difference between the two distributions is due to the finite size of the proton internal charge distribution. They are related by the convolution relation,

$$\rho_{\rm ch}(\vec{r}) = \int \rho_p(\vec{r}\,')\rho_{pfs}(\vec{r} - \vec{r}\,')d^3\vec{r}\,', \tag{10}$$

where $\rho_{pfs}(\vec{r})$ is the charge-density distribution of the proton. The experimental elastic electron-scattering data of a free proton can be well reproduced by the expression,

$$\rho_{pfs}(r) = \frac{1}{8\pi a^3}e^{-r/a}, \tag{11}$$

where $a^2 = \frac{1}{12}r^2_{pfs}$ with $r_{pfs} = 0.85$ fm being the corresponding charge root mean-square (rms) radius [12,13]. The Fourier transform of the charge density $\rho_{\rm ch}(\vec{r})$, determined by the

convolution relation of Eq. (10), is given by

$$F_{\rm ch}(q) = F_{pfs}(q)F_p(q), \tag{12}$$

where $F_{\rm ch}(q)$, $F_{pfs}(q)$, and $F_p(q)$, are the Fourier transforms of $\rho_{\rm ch}(\vec{r})$, $\rho_{pfs}(\vec{r})$, and $\rho_p(\vec{r})$, respectively. Equation (12) can be used to determine the form factor $F_p(q)$, associated with the point proton density distribution $\rho_p(r)$. Then $\rho_p(r)$ can be obtained from $F_p(q)$ by the inverse Fourier transform and compared with theoretical predictions.

III. RESULTS

In Fig. 1(a) we present (solid line) the experimental data [4,5] for the charge-density difference $\Delta\rho_c(r) = \rho_c(r;{}^{206}\text{Pb})\text{-}\rho_c(r;{}^{205}\text{Tl})$ between the isotones ^{206}Pb-^{205}Tl. It is normalized by the charge of one proton ($Z = 1$), and hence, it is replaced in the following by 1. The dotted lines indicate the limits of experimental uncertainty. The two maxima, such as those of the proton $3s_{1/2}$ orbit, are clearly seen in the figure. The experimental values of the charge rms radii of ^{206}Pb and ^{205}Tl are 5.4897 and 5.4792 fm, respectively, leading to a value of 6.2822 fm for the charge rms radius of the proton $3s_{1/2}$ orbit. To assess the possible rearrangement effect (from

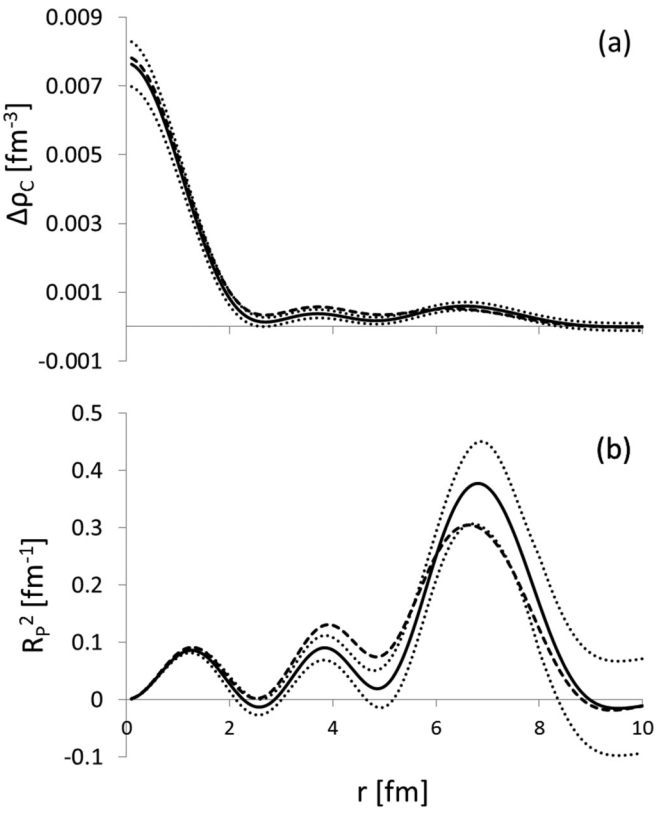

FIG. 1. (a) The experimental difference $\Delta\rho_c(r)$ between ^{206}Pb and ^{205}Tl charge distributions (solid line). The dashed line is for $\Delta\rho_{Rc}(r)$, the data after rearrangement correction. The dotted lines indicate the experimental uncertainty. (b) Similar to (a) for $R_p^2(r) = 4\pi r^2\Delta\rho_p(r)$ where $\Delta\rho_p(r)$ is derived from the experimental $\Delta\rho_c(r)$. The dashed line is for $R_{Rp}^2(r)$ related to $\Delta\rho_{Rp}(r)$ similarly obtained from $\Delta\rho_{Rc}(r)$.

^{205}Tl to ^{206}Pb) on the charge rms radius of the 81 core protons in ^{206}Pb, we assume that it increases by 0.005 fm, similar to the change between ^{206}Pb and ^{207}Pb [3]. The rearrangement effect is approximated (see Ref. [3]) by scaling the charge distribution of ^{205}Tl so that the charge rms radius of the scaled density is equal to that of the 81 core protons in ^{206}Pb. We thus obtain

$$\Delta\rho_{Rc}(r) = \rho_c(r;{}^{206}\text{Pb}) - \alpha^3\rho_c(\alpha r;{}^{205}\text{Tl}), \tag{13}$$

where the scaling parameter $\alpha = 5.4792/(5.4792 + 0.005) = 0.9990$ is the ratio between the charge rms radius of ^{205}Tl and that of the core 81 protons in ^{206}Pb. The form of (13) guarantees that the integral of $\Delta\rho_{Rc}(r)$ is equal to 1. The results for the charge density $\Delta\rho_{Rc}(r)$ are shown in Fig. 1(a) (dashed line).

To extract the corresponding single-particle potential using Eqs. (4) and (6) or (7), we need the point proton distribution $\Delta\rho_p(r)$. It is obtained by using Eqs. (11) and (12) to determine the point proton form factor $F_p(q)$ and then obtain $\Delta\rho_p(r)$ by inverse Fourier transform. Using the relation (5) we determined the values of $R_p^2(r) = 4\pi r^2\Delta\rho_p(r)$ as obtained from Fig. 1(a) and shown by the solid line in Fig. 1(b). If $\Delta\rho_p(r)$ is obtained from an eigenfunction of Eq. (1), $R_p(r)$ is related to it by (5). Similarly, $R_{Rp}^2(r) = 4\pi r^2\Delta\rho_{Rp}(r)$. The dashed line in Fig. 1(b) is obtained from the dashed line in Fig. 1(a). The dotted lines indicate the experimental uncertainty. We note that $R_p^2(r)$ as obtained from Fig. 1(a) (solid line) is slightly negative at the first node (at $\sim$2.6 fm) and above zero at the second node $r \sim 4.9$ fm. In Refs. [4,5] it was concluded that this result is consistent with the proton $3s_{1/2}$ orbit in the vicinity of these minima. However, the experimental uncertainty in $R_p^2(r)$ is larger than its value. The magnitude of the difference between $\Delta\rho_p(r)$ and $\Delta\rho_{Rp}(r)$ is similar to that of the experimental uncertainty.

We tried to use the experimental $R_p^2(r)$ and $R_{Rp}^2(r)$ of Fig. 1(b), shown by the solid and dashed lines, respectively, to directly deduce the corresponding potentials by employing (4) and (6). The Coulomb potential of Eq. (9) with $R_{\rm ch} = 7.1$ fm was adopted in the calculations. For nonsingular potential V, the second derivative $\frac{d^2R}{dr^2}$ should vanish when $R(r) = 0$. As seen from Fig. 1(b), this condition is not fulfilled at the minima of the experimental $R_p^2(r)$. Moreover, in the vicinity of the minima, in the regions of $r = 2.0 - 3.0$ and $r = 4.5 - 5.5$ fm, the uncertainty in $\Delta\rho_p(r)$ is larger than 50% of its value. Due to the large uncertainties in the experimental data, no reliable potential can be extracted.

Therefore, we considered several nuclear central potentials with the given Coulomb potential (9) added to each. We looked for potentials whose $3s_{1/2}$ wave functions yield charge distributions which fit best the measured one. The parameters of these potentials are obtained by least-squares fits of the calculated $R_p^2(r)$ to the corresponding experimental data. The fitted potential $V_F(r)$ is obtained by taking the values of the potential at the points $r = 3$, 6, and 9 fm as free parameters. The value of $V_F(0)$ is constrained to reproduce the experimental value of 7.25 MeV for the separation energy of the proton in the $3s_{1/2}$ orbit of ^{206}Pb. The value of $V_F(12)$ is taken to be zero. The values of $V_F(r)$ between these points are determined by polynomial interpolation (solid line in

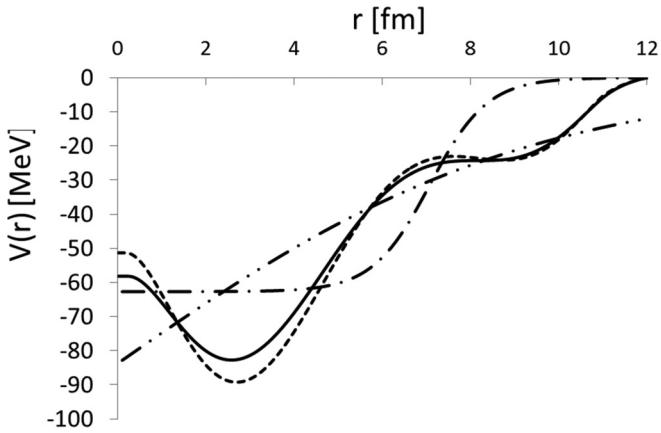

FIG. 2. Potentials fitted to data in Fig. 1(b). The $V_F(r)$ potential (solid line), the $V_{\rm FR}(r)$ version including rearrangement (dashed line), and the fitted $V_{\rm WSF}(r)$ potential (double-dotted-dashed line). Also shown is the conventional Woods-Saxon $V_{\rm WS}(r)$ potential (dashed-dotted line).

Fig. 2). From a fit to the experimental data of $R_p^2(r)$, the solid line in Fig. 1(b), we obtained the values of the parameters of $V_F(r)$ given in Table I. Similarly, the potential $V_{\rm RF}(r)$ (dashed line) is obtained by a fit to $R_{Rp}^2(r)$ [dashed line in Fig. 1(b)] with values of the parameters shown in Table I. The potential $V_{{\rm WS}F}(r)$, dashed-double-dotted line, is obtained by fitting the Woods-Saxon potential (8) to $R_p^2(r)$. The values of its parameters are given in Table I. For comparison, a conventional Woods-Saxon potential $V_{\rm WS}(r)$ is also shown by the dashed-dotted line with the values of its parameters given in Table I.

In Figs. 3(a) and 3(b), the experimental data of $R_c^2(r) = 4\pi r^2 \Delta\rho_c\,(r)$ and of $\Delta\rho_c\,(r)$ (between the two dotted lines) are compared with results of the proton $3s_{1/2}$ orbit. The latter were obtained from the potentials described above and shown in Fig. 2. The agreement between the experimental values and the results of the fitted $V_F(r)$ potential (solid line) is fair with $\chi^2/N = 1.15$. The results of the potential $V_{\rm RF}(r)$ (not shown in Fig. 3) are also in fair agreement with the data $\chi^2/N = 1.81$. The results of the fitted potential $V_{\rm WSF}(r)$, (dashed-double-dotted line) are also in reasonable agreement with the data $\chi^2/N = 3.28$. For comparison, we also show

TABLE I. Values of parameters of the standard WS potential and the fitted potentials.

	$V_{\rm WS}$	$V_{\rm WSF}$	V_F	$V_{\rm RF}$
χ^2/N	8.85	3.28	1.15	1.81
V_0 (MeV)	− 62.712	− 167.95		
R_1 (fm)	7.087	− 0.03		
a_0 (fm)	0.65	4.68		
$V(0)$ (MeV)			− 58.19	− 51.33
$V(3)$ (MeV)			− 81.35	− 88.29
$V(6)$ (MeV)			− 34.50	− 33.64
$V(9)$ (MeV)			− 23.54	− 23.96
$V(12)$ (MeV)			0.00	0.00

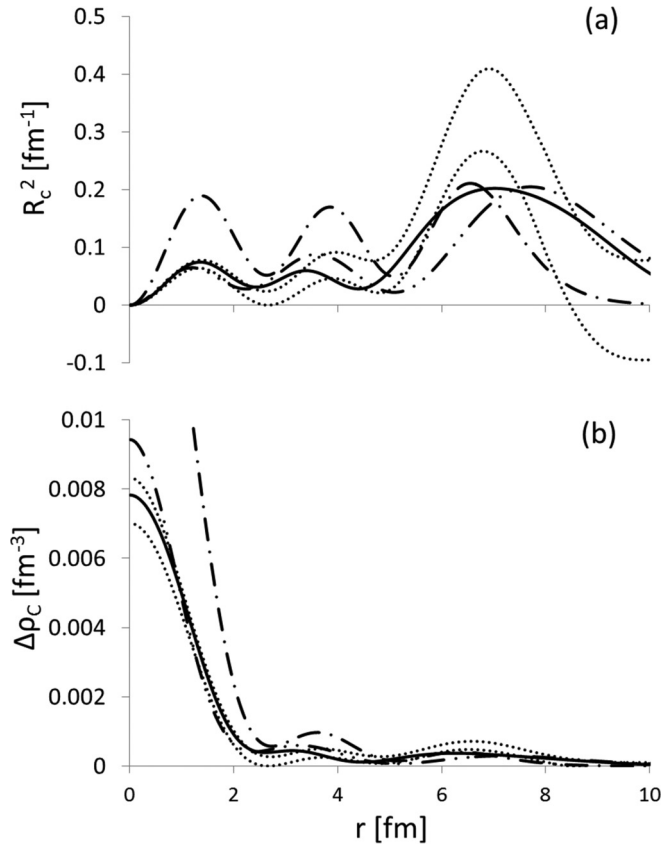

FIG. 3. Experimental values of (a) $R_c^2(r) = 4\pi r^2 \Delta\rho_c\,(r)$ and (b) $\Delta\rho_c\,(r)$ plotted between dotted lines of error limits. They are compared to calculated charge distributions due to the $3s_{1/2}$ wave functions of the fitted $V_F(r)$ potential (solid lines), the fitted Woods-Saxon $V_{\rm WSF}(r)$ potential (double-dotted-dashed lines), and the conventional $V_{\rm WS}(r)$ potential (dashed-dotted lines).

by the dashed-dotted line the results of the conventional Woods-Saxon potential $V_{\rm WS}(r)$. The agreement is much poorer with the value of $\chi^2/N = 8.85$.

The potential well of the shell model may well depend on the mass number A. It may also be nonlocal and depend on l. Still, it is interesting to look at the charge distribution due to the proton s orbits occupied in ^{206}Pb. They are the only orbits which contribute to the point proton density distribution at $r = 0$. In Figs. 4(a)–4(c) we compare the charge density of the $1s_{1/2}$, $2s_{1/2}$, and $3s_{1/2}$ proton orbits, respectively, obtained from the fitted potential $V_F(r)$ (solid lines) with those obtained from the conventional Woods-Saxon potential $V_{\rm WS}(r)$ (dashed-double-dotted line). The calculated contribution to $\rho_{\rm ch}(0)$ of the $s_{1/2}$ proton orbits for the fitted potential $V_F(r)$ is 0.053 fm^{-3}, significantly smaller than the value of 0.073 fm^{-3} obtained from the conventional Woods-Saxon potential $V_{\rm WS}(r)$, leading to a better agreement with the experimental observation of $\rho_{\rm ch}(0) = 0.063$ for ^{206}Pb [4,5,13]. The separation energies of the $1s_{1/2}$, $2s_{1/2}$, and $3s_{1/2}$ proton orbits are −47.09, −22.64, and −7.24 MeV for the $V_F(r)$ potential and −36.31, −24.46, and −8.00 MeV for the $V_{\rm WS}(r)$ potential, respectively. The relatively large separation energy of the $1s_{1/2}$ proton orbit

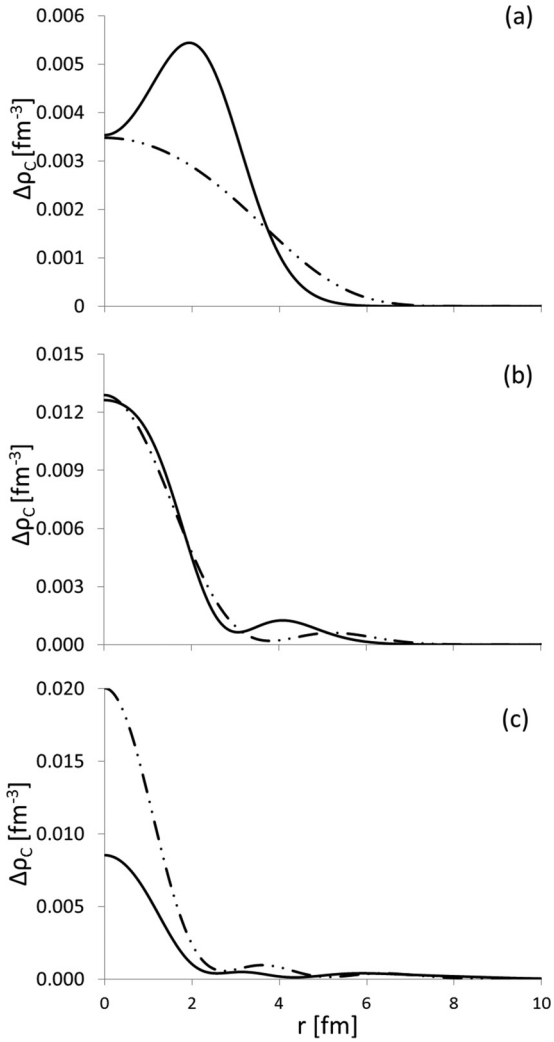

FIG. 4. Calculated charge densities of a proton in the (a) $1s_{1/2}$, (b) $2s_{1/2}$, and (c) $3s_{1/2}$ orbits in the $V_F(r)$ potential (solid lines) and the conventional $V_{\rm WS}(r)$ potential (double-dotted-dashed lines).

obtained for the $V_F(r)$ is close to the experimental value of −64.8 MeV [14].

IV. CONCLUSION

The difference between the charge distributions of ^{206}Pb and ^{205}Tl was measured many years ago. It offers a good opportunity to study possible effects of short-range correlations on the shell-model wave function of a proton in the $3s_{1/2}$ orbit. Effects of this kind were estimated by comparing measured cross sections of various reactions to those calculated using shell-model wave functions. Usually, the measured values were lower than the calculated ones. This depletion was sometimes attributed to effects of short-range correlations. The difference between the charge distributions considered here cannot be depleted. The integrated difference between charge densities must be exactly equal to the charge difference between the two isotones, one proton charge. The effects of short-range correlations in this case can only change the *shape* of the difference between the charge distributions.

The experimental values of that difference have features which are very similar to those due to the wave function of a proton in some $3s_{1/2}$ orbit. These are two zero values for $r > 0$ which correspond to the two nodes of the $3s$ wave function $R(r)/r$. If the point proton distribution $\rho_p(r)$ is due to a $3s$ wave function, two conditions should be satisfied in addition to its having first and second derivatives for all r values. These conditions are presented after Eq. (7). They are necessary to derive the single nucleon potential using (4), (6), or (7) from a proton distribution $\rho_p(r)$. It is difficult to see whether these conditions are satisfied by the measured difference of charge distributions. The experimental accuracy is not sufficient, particularly near the zero values.

We started by deriving and employing a new relation [11] between the potential V and the single-particle density and its first and second derivatives. Due to insufficient experimental accuracy, no reliable potential can be obtained in this way. In view of this situation, we tried to construct a nuclear single-particle potential V whose proton $3s_{1/2}$ orbit in ^{206}Pb yields charge distributions which best fit the electron-scattering results [4,5]. We found several potentials which yield fair fits to the data (Fig. 3). The fair agreement with fitted potentials may be an indication that effects of short-range correlations on charge distributions of shell-model wave functions are not significant. Still, to answer the question to what extent the data agree with the distribution due to a $3s$ wave function of some potential, better accuracy of the measurement is needed. The uncertainty in values of $\Delta\rho_c(r)$ must be reduced by a factor of 2 or more before an accurate determination of the effects of short-range correlations on shell-model wave functions can be achieved. This is a strong demand on the plan of experiments described in Ref. [15].

ACKNOWLEDGMENTS

S.S. would like thank The Weizmann Institute of Science for the kind hospitality. This work was supported, in part, by the U.S. Department of Energy under Grant No. DOE-FG03-93ER40773.

[1] N. Antonov, P. E. Hodgson, and I. Z. Petkov, *Nucleon Momentum and Density Distributions in Nuclei* (Clarendon, Oxford, 1988); *Nucleon Correlations in Nuclei* (Springer-Verlag, Berlin/Heidelberg/New York, 1993).

[2] V. R. Pandharipande, I. Sick, and P. K. A. deWitt Huberts, Rev. Mod. Phys. **69**, 981 (1997).

[3] H. Euteneuer, J. Friedrich, and N. Voegler, Nucl. Phys. A **298**, 452 (1978).

[4] J. M. Cavedon *et al.*, Phys. Rev. Lett. **49**, 978 (1982).

[5] B. Frois *et al.*, Nucl. Phys. A **396**, 409c (1983).
[6] L. S. Celenza, A. Harindranath, and C. M. Shakin, Phys. Rev. C **32**, 2173 (1985).
[7] S. V. Akulinichev, S. Shlomo, S. A. Kulagin, and G. M. Vagradov, Phys. Rev. Lett. **55**, 2239 (1985).
[8] I. Stetcu, B. R. Barrett, P. Navratil, and J. P. Vary, Phys. Rev. C **71**, 044325 (2005).
[9] S. Shlomo, in *The Universe Evolution: Astrophysical and Nuclear Aspects,* edited by L. Blokhintsev and I. Strakovsky (Nova Science, New York, 2013).
[10] B. K. Agrawal, S. Shlomo, and V. K. Au, Phys. Rev. C **72**, 014310 (2005).
[11] S. Shlomo and M. R. Anders, Phys. Atom. Nucl. (to be published).
[12] L. R. B. Elton, *Nuclear Sizes* (Oxford University Press, London, 1961).
[13] H. De Vries, C. W. De Jager, and C. de Vries, At. Data Nucl. Data Tables **36**, 495 (1987).
[14] A. A. Vorobev, Y. V. Dotsenko, A. A. Lobodenko, O. V. Miklukho, I. I. Tkach, A. Y. Tsaregorodtsev, and Y. A. Shcheglov, Phys. At. Nucl. **58**, 1817 (1995).
[15] A. N. Antonov *et al.*, Nucl. Instrum. Methods Phys. Res., Sect. A **637**, 60 (2011).